Current injection into a two-dimensional anisotropic bidomain

Nestor G. Sepulveda, Bradley J. Roth, and John P. Wikswo, Jr.
Living State Physics Group, Department of Physics and Astronomy, Vanderbilt University, Nashville, Tennessee 37235

ABSTRACT A two-dimensional sheet of anisotropic cardiac tissue is represented with the bidomain model, and the finite element method is used to solve the bidomain equations. When the anisotropy ratios of the intracellular and extracellular spaces are not equal, the injection of current into the tissue induces a transmembrane potential that has a complicated spatial dependence, including adjacent regions of depolarized and hyperpolarized tissue. This behavior may have important implications for the electrical stimulation of cardiac tissue and for defibrillation.

INTRODUCTION

To better understand the electrical stimulation of cardiac muscle and defibrillation, we must determine how cardiac tissue responds to externally applied currents. In this paper we use the bidomain model and the finite element method to calculate the electrical response of a two-dimensional sheet of cardiac muscle to point current sources. We find that, in general, anisotropic cardiac tissue responds to an applied current by producing a spatially complicated distribution of potential and current, including adjacent depolarized and hyperpolarized regions.

The electrical behavior of cardiac muscle is represented using the bidomain model, a macroscopic model that describes the average behavior of the bioelectric fields over distances that are large compared with the size of a single cell. In the bidomain model, cardiac tissue is represented by two superimposed but distinct continuous domains, intracellular and interstitial, separated everywhere by the cell membrane. The anisotropic electrical properties of both the intracellular and interstitial domains are characterized by their electrical conductivity tensors. Although the bidomain model describes only the macroscopic behavior of syncytial tissue, it has been used to explain measurements of passive current flow in the lens of the eye (1), cable constant measurements (2) and intracellular resistivity measurements (3) in strands of cardiac tissue, the electrocardiogram (4, 5), the magnetocardiogram (6), four-electrode resistivity measurements (7), and extracellular measurements of the electric potentials produced by two-dimensional propagation in atrial or ventricular muscle (8–11).

In a previous paper we investigated the potential, current, and magnetic field produced by a depolarization wavefront propagating radially through a two-dimensional sheet of anisotropic bidomain tissue (11). The goal of our present work is to determine the extracellular, intracellular, and transmembrane potential distributions resulting from the injection of current into the same tissue. This calculation is fundamentally important, because passive cardiac tissue is a linear system and therefore the response of cardiac tissue to any applied current can be represented by a superposition of its response to point current sources. Determining the transmembrane potential from a current source is a more difficult problem than determining the intracellular and extracellular potentials from a given transmembrane potential (11), because in the former calculation the bidomain equations do not uncouple, whereas in the latter they do. Our approach uses the finite element method to solve simultaneously the coupled bidomain equations.

METHODS

The bidomain model is expressed mathematically by a pair of coupled partial differential equations, which have been solved analytically in some special cases (7, 12–14). The general steady-state equations governing the electrical potentials are

$$\nabla \cdot \tilde{\tilde{\sigma}}_i \nabla \phi_i = I_m + f_{is} \tag{1}$$

$$\nabla \cdot \tilde{\tilde{\sigma}}_e \nabla \phi_e = -I_m + f_{es}, \tag{2}$$

where ϕ_i and ϕ_e are the potentials in the intracellular and extracellular domains, $\tilde{\tilde{\sigma}}_i$ and $\tilde{\tilde{\sigma}}_e$ are the conductivity tensors describing the anisotropic intracellular and extracellular conductive media, I_m is the transmembrane current per unit volume, and f_{is} and f_{es} are the externally applied intracellular and extracellular current per unit volume, respectively.

Dr. Roth's current address is Biomedical Engineering and Instrumentation Branch, Division of Research Services, National Institutes of Health, Bethesda, MD 20892.

0006-3495/89/05/987/13 $2.00

Under steady-state conditions the transmembrane current, I_m, is given by

$$I_m = (\beta/R_m)\,\phi_m, \tag{3}$$

where R_m is the membrane resistance times unit area ($\Omega \cdot m^2$), β is the ratio of the membrane surface area to the volume occupied by the tissue (surface-to-volume ratio, m^{-1}), and ϕ_m is the transmembrane potential,

$$\phi_m = \phi_i - \phi_e. \tag{4}$$

Because the tissue is assumed to be passive, R_m is not a function of the transmembrane potential.

We consider a two-dimensional anisotropic bidomain which is infinite in extent. In a rectangular coordinate system (x, y), Eqs. 1 and 2 are written as

$$\sigma_{ix}\partial^2\phi_i/\partial x^2 + \sigma_{iy}\partial^2\phi_i/\partial y^2 - (\beta/R_m)\,\phi_i + (\beta/R_m)\,\phi_e = f_{is} \tag{5}$$

$$\sigma_{ex}\partial^2\phi_e/\partial x^2 + \sigma_{ey}\partial^2\phi_e/\partial y^2 - (\beta/R_m)\,\phi_e + (\beta/R_m)\,\phi_i = f_{es}. \tag{6}$$

Here we have assumed that the bidomain conductivities are uniform throughout the tissue (they are not functions of x and y), and that the principle axes of both of the conductivity tensors lie along the x and y axes. Given the appropriate boundary conditions and the applied current sources, we can solve Eqs. 5 and 6 to determine the intracellular and extracellular potentials. Once these potentials are known, the transmembrane potential distribution may be calculated using Eq. 4. The bidomain conductivities, the membrane resistance times unit area, and the surface-to-volume ratio are the key factors determining the electrical behavior of the tissue. Thus far, a precise quantification of these parameters based upon the microscopic electrical properties of the tissue and the cellular microstructure has not been performed. Until these data become available, we use measured values of the conductivities which have been used in previous calculations (7, 15).

Whereas Eqs. 5 and 6 have not been solved analytically in their most general form, an analytical solution for the transmembrane potential can be obtained for the special case of equal anisotropy ratios ($\sigma_{ix}/\sigma_{ex} = \sigma_{iy}/\sigma_{ey}$). If a current source of magnitude I_o (A m^{-1}) is applied cathodally to the extracellular domain at the origin of the coordinate system, so that

$$f_{es} = -I_o\,\delta(x)\,\delta(y) \tag{7}$$

and

$$f_{is} = 0, \tag{8}$$

then the induced transmembrane potential is

$$\phi_m = \frac{I_o}{2\pi\sqrt{\sigma_{ey}\sigma_{ex}}}\,K_0(r/\lambda), \tag{9}$$

where $r = \sqrt{x^2 + \kappa y^2}$, $\kappa = \sigma_{ex}/\sigma_{ey}$, the length constant λ is given by

$$\lambda = \sqrt{\frac{R_m}{\beta(1/\sigma_{ix} + 1/\sigma_{ex})}}, \tag{10}$$

and $K_0(r/\lambda)$ is the modified Bessel function of the second kind of order zero. This solution is analogous to that derived by Woodbury and Crill (16) when studying current injection into the atrium.

If at the origin there are two point sources of equal magnitude and opposite sign, one in the intracellular domain and the other in the extracellular domain, so that

$$f_{is} = I_o\,\delta(x)\,\delta(y) \tag{11}$$

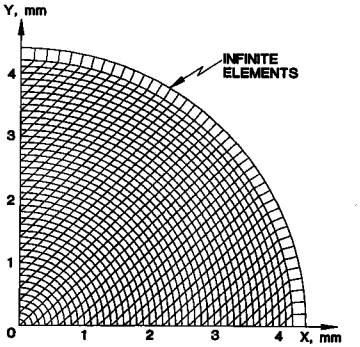

FIGURE 1 The finite element grid used in these calculations. Grid consists of 882 isoparametric quadrilateral eight-node elements, 42 isoparametric triangular six-node elements, and 42 infinity elements. Total number of nodes is 2,985. Each node has two degrees of freedom (ϕ_i and ϕ_e).

and

$$f_{es} = -I_o\,\delta(x)\,\delta(y), \tag{12}$$

then

$$\phi_m = \frac{\sqrt{\kappa}\,I_o}{2\pi}\left(\frac{1}{\sigma_{ix}} + \frac{1}{\sigma_{ex}}\right)K_0(r/\lambda). \tag{13}$$

These results are useful for testing our numerical calculation.

In general the bidomain equations are difficult to solve analytically, and numerical techniques must be used (9–11). We use the finite element method, which is a well-established numerical technique for solving partial differential equations (17–20). In our previous paper (11), the transmembrane potential was specified everywhere, so that Eqs. 5 and 6 could be decoupled and solved separately. In the present problem, we are determining the transmembrane potential distribution for known injected currents. In this case the two equations are coupled and they must be solved simultaneously.

For our calculation we have used a circular block of cardiac tissue of infinite extent, similar to that used by Sepulveda and Wikswo (11). Because the model has symmetric geometry, conductivity properties, and boundary conditions, we only need to analyze one quarter of the region. A finite element grid of standard eight-node quadrilateral and

TABLE 1 Tissue properties

Conductivity	Equal anisotropy ratio	Nominal anisotropy	Reciprocal anisotropy
S/mm			
σ_{ix}	3.43×10^{-4}	2×10^{-4}	2×10^{-4}
σ_{iy}	5.96×10^{-5}	2×10^{-5}	2×10^{-5}
σ_{ex}	6.25×10^{-4}	8×10^{-4}	2×10^{-5}
σ_{ey}	1.09×10^{-4}	2×10^{-4}	2×10^{-4}

Membrane resistance times unit area, R_m = 200,000 Ohms-mm^2. Surface-to-volume ratio, β = 200 mm^{-1}. Data from references 7 and 10.

TABLE 2 Comparison of analytic and finite element solutions

Distance ($y = 0.0$)	Analytical value	Finite element solution	Difference
x (mm)	*mV*	*mV*	*%*
0.10	4135.75	4162.05	−0.635
0.30	1783.48	1782.41	0.060
0.50	940.83	935.63	0.552
1.00	238.90	238.72	0.072
1.50	68.45	68.22	0.338
2.00	20.66	20.63	0.139
2.50	6.42	6.42	0.063
3.00	2.03	2.03	−0.140

Cathodal current is applied extracellularly at the origin, with strength $I_o = 4$ mA/mm. Return current at infinity.

six-node triangular isoparametric elements was automatically generated in a circular region of radius equal to 4.2 mm. At the outer border of the circular region a layer of "infinity" elements was also generated to account for the boundary conditions at infinity. The finite element grid is shown in Fig. 1 and has 42 six-node triangles, 882 eight-node quadrilateral and 42 infinity elements. We consider two different applied current sources. First, a point current source is located in the extracellular space at the origin, and current flows from the source to infinity. Second, two point current sources are located at the origin, one in the intracellular space and the other of equal magnitude and opposite sign in the extracellular space, so that current entering the tissue from one electrode leaves the tissue through the other electrode.

The values for the bidomain conductivities were obtained from Plonsey and Barr (7, 10), and are summarized in Table 1. We consider three sets of conductivity values: equal anisotropy ratios, with which we also obtained analytic solutions; nominal values, corresponding to values measured experimentally for cardiac muscle; and reciprocal anisotropy, in which case $\sigma_{ix}/\sigma_{iy} = \sigma_{ey}/\sigma_{ex}$, so the direction of high conductivity in the intracellular and extracellular domains are perpendicular. The rather extreme case of reciprocal anisotropy is of interest because it was

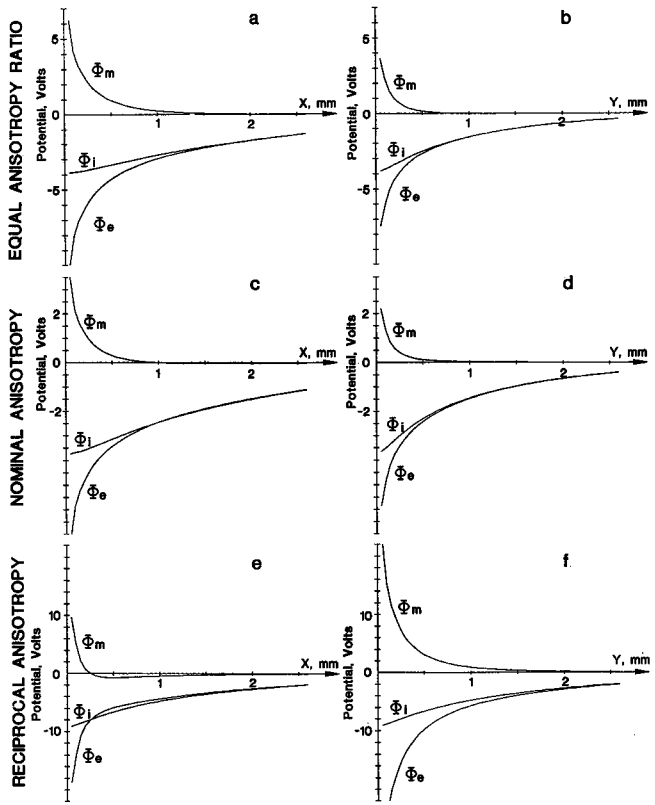

FIGURE 2 The calculated electrical potentials for different conductivities. The intracellular (ϕ_i), extracellular (ϕ_e), and transmembrane (ϕ_m) potentials are shown as functions of the distance along either the x- or y-axis, for equal anisotropy ratios (a, b), nominal (c, d), and reciprocal conductivities (e, f). The current is cathodally applied with an extracellular electrode at the origin, with strength $I_o = 4$ mA/mm.

examined by Muler and Markin (8), and thus that work provides a check for our results. Furthermore, the reciprocal case also has a symmetry between the intracellular and extracellular spaces that leads to symmetries in the predicted potential, current, and magnetic field distributions. These symmetries thereby provide an additional check as to the validity of our numerical calculations. The value of R_m and β were taken from Plonsey and Barr (7).

RESULTS

As a test of our calculation, we examine the case of equal anisotropy ratios and a single point current source in the extracellular space at the origin. In Table 2 we compare the analytic expression for the transmembrane potential given in Eq. 9 with the solution obtained using the finite element method for a few points along the x-axis.

In Fig. 2 we show that calculated extracellular, intracellular, and transmembrane potentials as functions of distance from the current source along the x- and y-axes, for equal anisotropy ratios, nominal, and reciprocal conductivities. In all cases, the transmembrane potential falls off with distance more rapidly than do the intracellular and extracellular potentials. For nominal conductivities there is a crossover of the transmembrane potential from positive to negative values along the x-axis at a distance of ~1.5 mm, and for the case of reciprocal conductivities a crossover occurs at ~0.3 mm. This indicates the existence

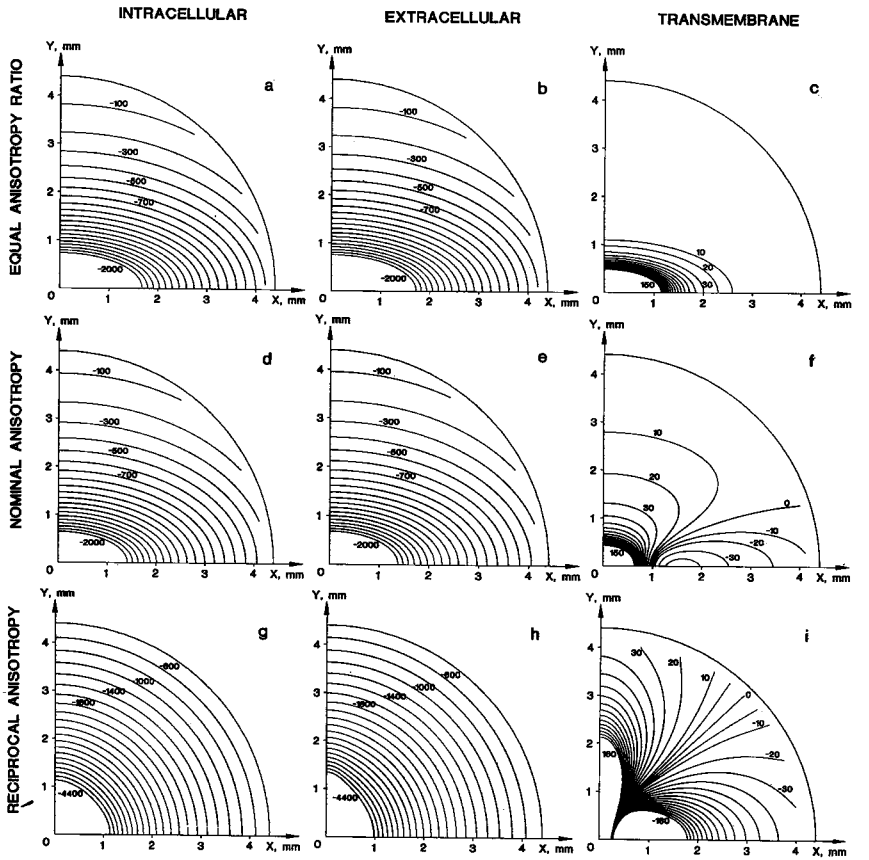

FIGURE 3 The calculated isopotential contours in millivolts for different conductivities. Intracellular, extracellular, and transmembrane isopotential contours are calculated for equal anisotropy ratios (*a–c*), nominal (*d–f*), and reciprocal conductivities (*g–i*). The current is cathodally applied with an extracellular electrode at the origin, with strength $I_o = 4$ mA/mm. The isopotential contours near the source become very close together, and are not drawn.

of adjacent regions that are depolarized and hyperpolarized simultaneously by the injected current.

Fig. 3 depicts the calculated intracellular, extracellular, and transmembrane isopotential contours for the three sets of conductivities. In all cases, the intracellular and extracellular isopotential contours are roughly elliptical in shape. The transmembrane isopotential contours for equal anisotropy ratios also follow an elliptical pattern, as predicted by Eq. 9. For nominal conductivities the transmembrane isopotentials have an approximately elliptical shape for distances <0.7 mm. Farther away, the transmembrane exhibits a complicated spatial dependence. Note the presence of a relative minimum of the transmembrane potential along the x-axis. Similar behavior is also present in the transmembrane potential calculated using reciprocal conductivities. A three-dimensional plot of the transmembrane potential in these three cases is shown in Fig. 4, indicating more clearly the presence of the adjacent depolarized and hyperpolarized regions.

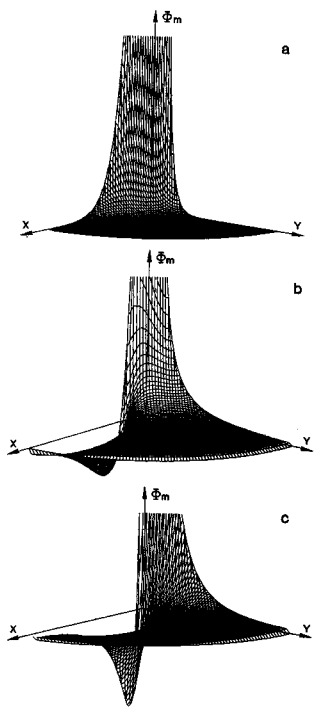

FIGURE 4 Corresponding three-dimensional plots of the transmembrane potentials presented in Fig. 3 (c, f, i).

Fig. 5 shows the calculated intracellular and extracellular current density, for equal anisotropy ratios, nominal, and reciprocal conductivities. Each vector indicates the direction of the current and the relative magnitude of the current with a logarithmic scale. If the intracellular and extracellular domains do not have equal anisotropy ratios, then the total current, as shown in Fig. 6, contains a component that forms closed loops. The presence of these loops is not obvious from Fig. 6, as they are masked by the larger current flowing inward toward the current source. These current loops have a profound effect on the magnetic field.

In Table 3 we compare the analytical expression for the transmembrane potential given by Eq. 13 and the calculated values for equal anisotropy ratio when there are two current sources at the origin, in the intracellular and extracellular domains. Fig. 7 shows the intracellular, extracellular, and transmembrane potentials along the x- and y-axes; Fig. 8 shows the intracellular, extracellular, and transmembrane isopotential contours produced by this source for all three sets of conductivity values; Fig. 9 shows three-dimensional plots of the transmembrane potentials; and Fig. 10 shows the current densities. For this source, the intracellular and extracellular potentials as well as the transmembrane potential have complex spatial dependencies if the intracellular and extracellular spaces do not have equal anisotropy ratios. Note from Fig. 11 that the total current forms closed loops.

In the reciprocal anisotropy case, there is complete symmetry of the transmembrane potential about a line 45° from the x- and y-axes. This particular simulation has also been studied by Muler and Markin (8). They used two-dimensional Fourier transform methods to solve the bidomain equations, but were unable to solve the Fourier integrals analytically for ϕ_m. We have used a two-dimensional fast Fourier transform routine (21) to evaluate numerically their Fourier integral expression for ϕ_m, and obtained results consistent with those obtained using the finite element technique. Muler and Markin found an analytic expression for the asymptotic behavior of the transmembrane potential at large radial distances, r (r and Θ are the polar coordinates in the x, y plane). Their expression implies that for all angles Θ, the transmembrane potential should be either always negative or always positive, but should not change sign. From Fig. 8i we see that at $r = 4$ mm our numerically calculated ϕ_m alternates sign with a rotation of Θ by 45°. It is not clear from our calculations whether the zero-potential lines, as seen in Fig. 8, meet at $\Theta = 45°$, at $\Theta = 0°$ and 90°, or never meet, which could cause ϕ_m to be everywhere positive at large r, everywhere negative, or alternate, respectively. We have taken our numerical calculations out to $r = 20$ mm, and the potential continues to alternate sign with Θ.

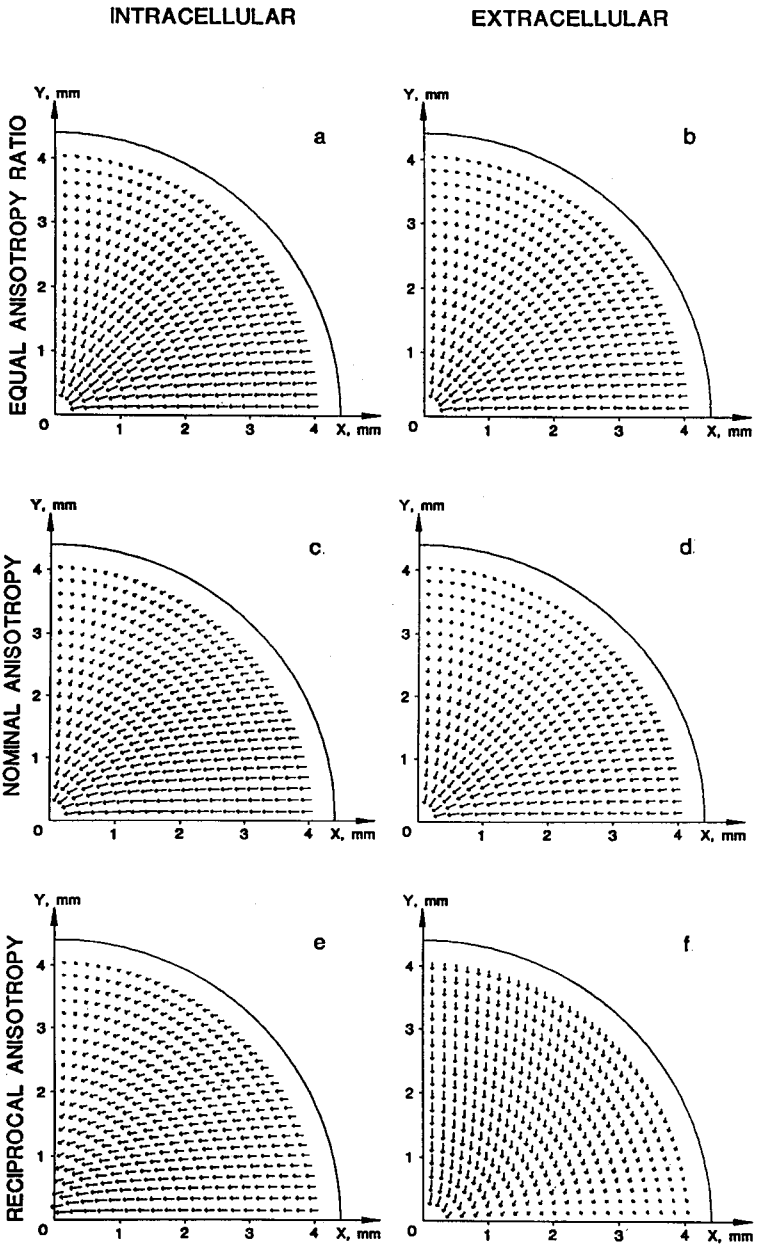

FIGURE 5 The calculated current density for different conductivities. The intracellular and extracellular current densities are calculated for equal anisotropy ratios (*a*, *b*), nominal (*c*, *d*), and reciprocal conductivities (*e*, *f*). The current is cathodally applied with an extracellular electrode at the origin, with strength $I_o = 4$ mA/mm. The length of the arrows depend logarithmically on the strength of the current density.

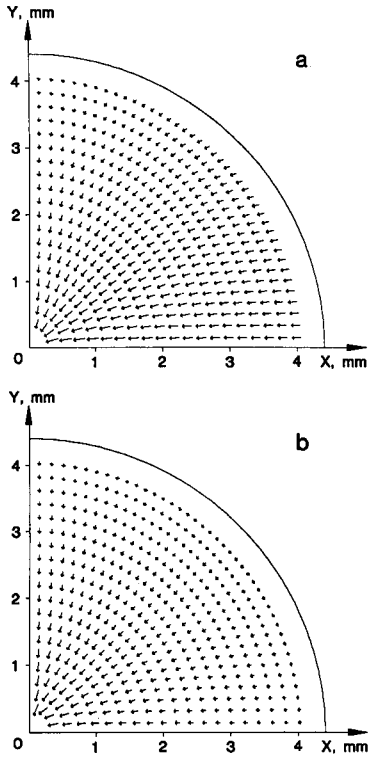

FIGURE 6 The calculated total (or net) current density for nominal (*a*) and reciprocal conductivities (*b*). Current is cathodally applied with an extracellular electrode at the origin, with strength I_o = 4 mA/mm. Length of arrows depend logarithmically on the strength of the current density.

TABLE 3 Comparison of analytic and finite element solutions

Distance (y = 0.0)	Analytical value	Finite element solution	Difference
x (mm)	*mV*	*mV*	*%*
0.10	11655.30	11729.50	−0.636
0.30	5026.18	5023.27	0.057
0.50	2651.45	2636.89	0.549
1.00	673.26	672.84	0.062
1.50	192.93	192.32	0.316
2.00	58.24	58.17	0.120
2.50	18.10	18.07	0.198
3.00	5.73	5.72	0.132

Current is applied at the origin, with intracellular and extracellular electrodes carrying current of equal strength but different sign, with strength I_o = 4 mA/mm.

It is possible, however, that at even larger values of r the transmembrane potential approaches Muler and Markin's asymptotic limit.

In the bidomain model, the potentials depend on five parameters: the four conductivities σ_{ix}, σ_{ex}, σ_{iy} and σ_{ey}, and the ratio of the surface-to-volume ratio β and the membrane resistance times unit area R_m. Using the Fourier integral formulation (8), it can be shown that $\sqrt{\beta/R_m}$ scales the radial distance r without otherwise changing the shape of the isopotential curves. For tissues with equal anisotropy ratios, the ratio $\kappa = \sigma_{ex}/\sigma_{ey}$ stretches the isopotential contours along either the x or y direction. Another combination of conductivities determines the amplitude of the potentials: $1/\sqrt{\sigma_{ey}\sigma_{ex}}$ in the case of a single current source, and $\sqrt{\kappa}\ (1/\sigma_{ix} + 1/\sigma_{ex})$ for two current sources.

To study how the potential distributions vary with the conductivities, other than the reciprocal values, we must perform numerical calculations. Figs. 12 and 8*f* show the transmembrane potential produced by current injection in both the intracellular and extracellular spaces, for the three sets of conductivity values presented in Table 4. Each set differs primarily in the anisotropy ratio of the intracellular and extracellular spaces. Note that as the anisotropy ratio increases, for both the intracellular and extracellular spaces, the shape and position of the hyperpolarized region changes.

If the anisotropy ratios of the intracellular and extracellular space are not equal then the total current may form closed loops, which in turn produce a magnetic field. Sepulveda and Wikswo (11) have calculated the magnetic field produced by a propagating action potential in a two-dimensional sheet of bidomain tissue. A similar magnetic field is produced by current injection into a two-dimensional bidomain. Isofield lines for the normal component of the magnetic field are shown in Fig. 13. The field pattern has a characteristic clover leaf shape, distinctive of an octapole source. The sign of the field pattern depends on the conductivities and it can be positive or negative in the first quadrant.

DISCUSSION

We have studied the behavior of anisotropic cardiac tissue using the bidomain model, solving the bidomain equations using the finite element method. Our results show that when the anisotropy ratios of the intracellular and extracellular spaces are not equal, the transmembrane potential produced by injecting current into a 2-D sheet of cardiac tissue has a complicated spatial dependence, and there exist adjacent depolarized and hyperpolarized regions.

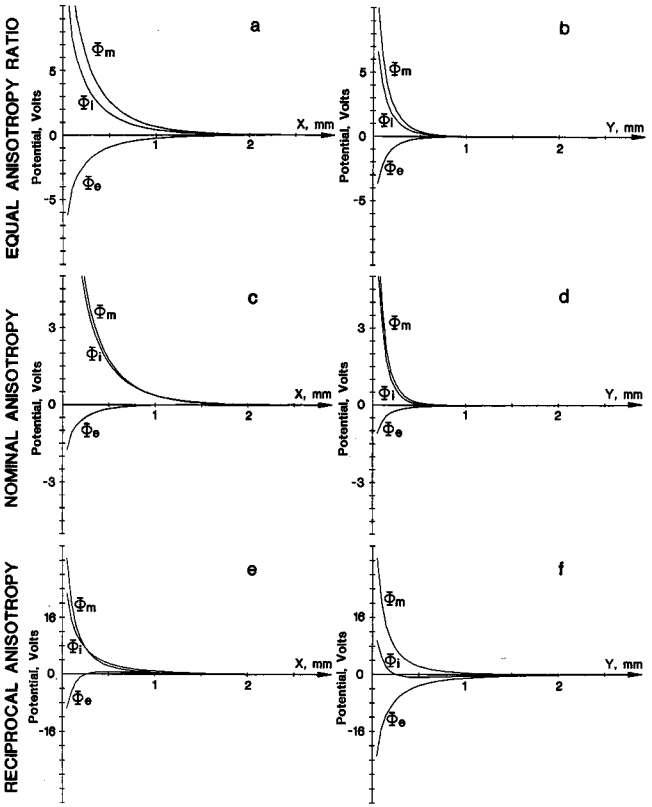

FIGURE 7 Calculated electrical potentials for different conductivities. Intracellular (ϕ_i), extracellular (ϕ_e), and transmembrane (ϕ_m) potentials are shown as functions of the distance along either the x- or y-axis, for equal anisotropy ratios (a, b), nominal (c, d), and reciprocal conductivities (e, f). The current is applied at the origin, with the intracellular electrode (+) and extracellular electrode (−) carrying equal and opposite currents with strength I_o = 4 mA/mm.

As an example of how these effects might affect cardiac stimulation and propagation, consider the stimulation of a cardiac action potential by a point current electrode. Let us assume that an action potential will be initiated wherever our model predicts that the transmembrane potential is depolarized by +20 mV or more. Using equal anisotropy ratios, nominal, and reciprocal conductivities, Fig. 14 shows the +20 mV isopotential line for increasing stimulation current. This isopotential line represents the edge of the "virtual cathode," or the edge of the region of tissue stimulated by the applied current (22, 23). For nominal and reciprocal anisotropies not only the size but also the shape of the virtual cathode changes dramatically with increasing current. At low currents, the virtual cathode is approximately elliptical in shape, with the principal axis of the ellipse transverse to the fiber direction. At large currents it takes on a more "dumbbell" or "dogbone" shape. Preliminary experimental data is in general agreement with this prediction (manuscript in preparation). Interestingly, if the sign of the current is changed, so that we have a positive electrode or anode at the origin, we can still produce depolarization of the tissue; the virtual cathode still exists, as seen in Fig. 14, but now in the form of ellipses, on either side of the stimulus site, displaced from the origin along the fiber axis.

This calculation also has implications for cardiac defibrillation. We show that in the nominal case, the transmembrane potential produced by injecting current into cardiac muscle can have a very complicated pattern, with

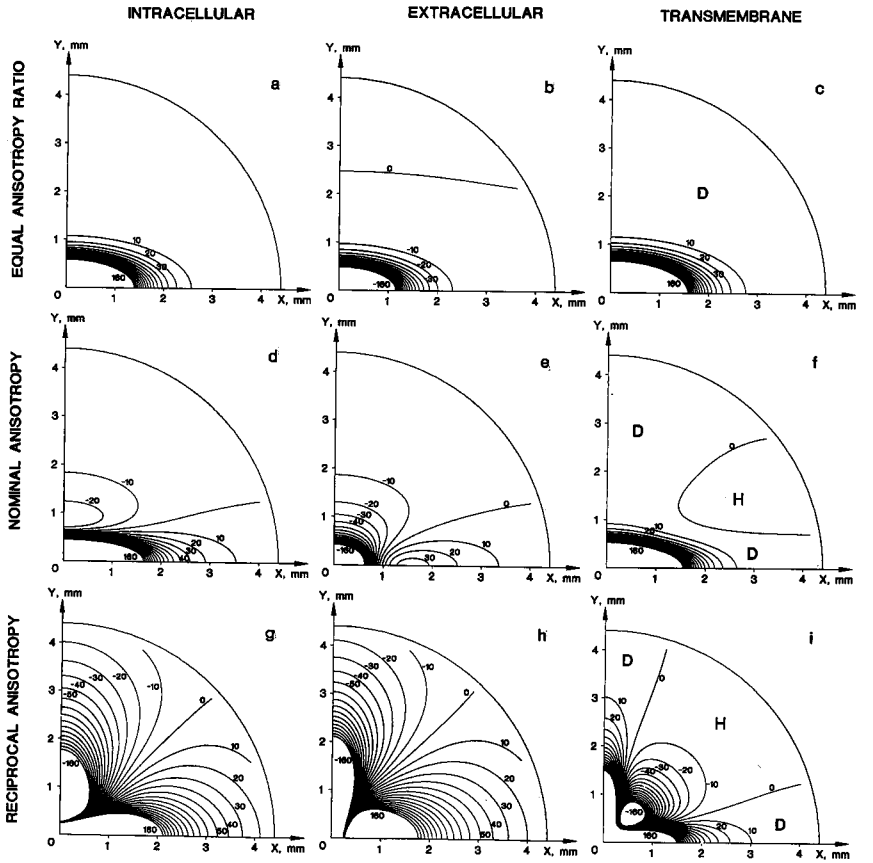

FIGURE 8 The calculated isopotential contours in millivolts for different conductivities. The intracellular (ϕ_i), extracellular (ϕ_e), and transmembrane (ϕ_m) isopotential lines are calculated for equal anisotropy ratios (*a–c*), nominal (*d–f*), and reciprocal conductivities (*g–i*). The current is applied at the origin, with the intracellular electrode (+) and the extracellular electrode (−) carrying equal and opposite currents with strength $I_o = 4$ mA/mm.. The isopotential lines near the source become very close together, and are not drawn. In panels *c*, *f*, and *i*, labels *D* and *H* identify the regions where the intracellular space is depolarized and hyperpolarized, respectively.

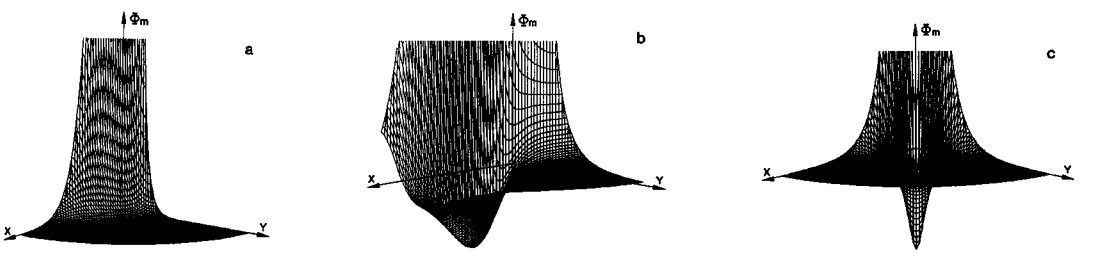

FIGURE 9 Corresponding three-dimensional plots of the transmembrane potentials presented in Fig. 8, *c*, *f*, *i*.

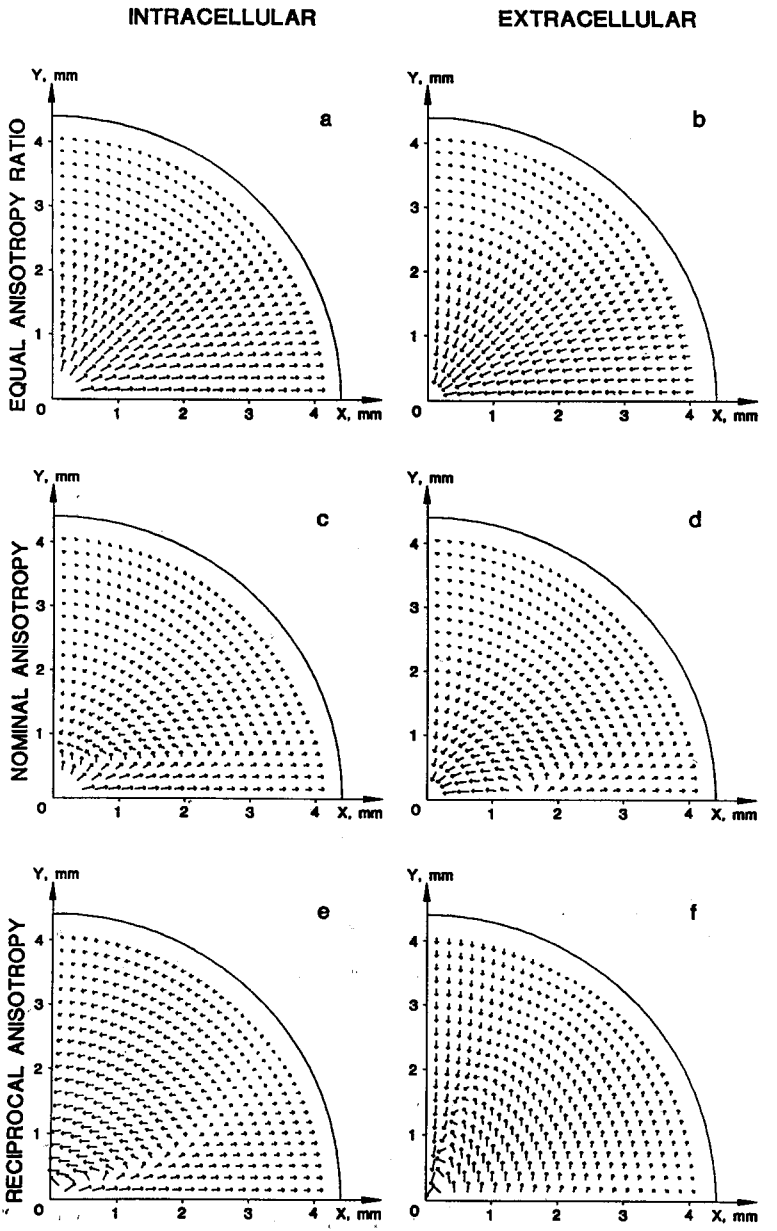

FIGURE 10 Calculated current density for different conductivities. Intracellular (J_e) and extracellular (J_3) current densities are calculated for equal anisotropy ratios (*a*, *b*), nominal (*c*, *d*), and reciprocal (*e*, *f*) conductivities. The current is applied at the origin, with the intracellular electrode (+) and the extracellular electrode (−) carrying equal and opposite currents with strength I_e = 4 mA/mm. The length of the arrows depends logarithmically on the strength of the current density.

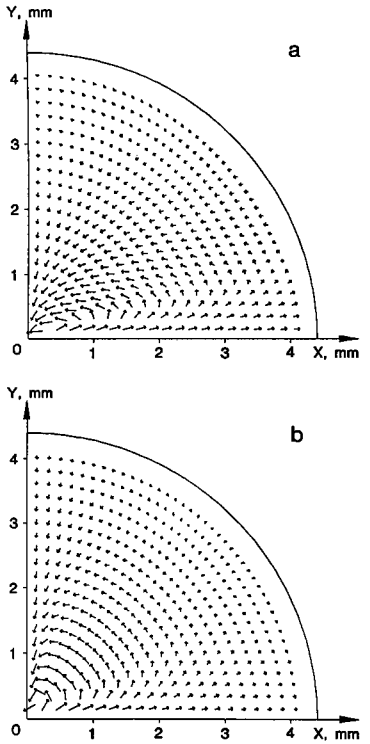

FIGURE 11 Calculated total (or net) current density for nominal (*a*) and reciprocal conductivities (*b*). The current is applied at the origin, with intracellular and extracellular electrodes carrying current of equal strength but different sign, with strength I_o = 4 mA/mm. Length of arrows depends logarithmically on the strength of the current density.

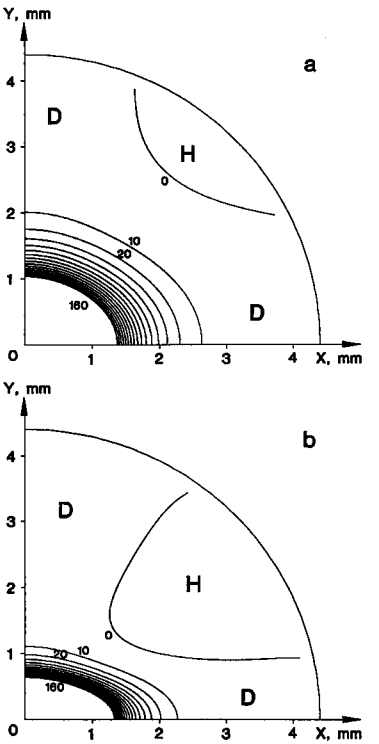

FIGURE 12 The transmembrane isopotentials for different anisotropy ratios. The potential was calculated using the conductivity values listed in Table 4. In each calculation, R_m = 200,000 Ohms-mm^2 and β = 200 mm^{-1}. Panels *a* and *b* correspond to Columns I and III in Table 4. The intermediate case of nominal anisotropy is shown in Fig. 8*f* and column II of Table 4. The current is applied at the origin, with the intracellular (+) and the extracellular electrodes (−) carrying current of equal strength but different sign, with strength I_o = 4 mA/mm. The labels *D* and *H* identify the regions where the intracellular space is depolarized and hyperpolarized, respectively.

both depolarized and hyperpolarized regions. This indicates that both the anisotropy of the intracellular and extracellular spaces must be taken into account before the transmembrane potential distribution from externally applied current can be predicted accurately.

The magnetic field is zero unless the intracellular and interstitial domains have different anisotropy ratios. Thus, measurement of the magnetic field offers a sensitive technique to detect differences in the anisotropy ratios by determining whether there exist any current loops that are associated with unusual transmembrane potential distributions arising from unequal anisotropy ratios. It may also be possible to use simultaneous measurements of the potential and magnetic field to determine the conductivity of the tissue (11). These effects are well within the capabilities of high-resolution magnetometers (24).

TABLE 4 Conductivity values to study changes in anisotropy ratio

Conductivity	I	II*	III
S/mm			
σ_{ix}	1.5×10^{-4}	2.0×10^{-4}	3.0×10^{-4}
σ_{iy}	0.3×10^{-4}	0.2×10^{-4}	0.15×10^{-4}
σ_{ex}	6.0×10^{-4}	8.0×10^{-4}	12.0×10^{-4}
σ_{ey}	3.0×10^{-4}	2.0×10^{-4}	1.5×10^{-4}
Anisotropy ratio			
σ_{ix}/σ_{iy}	5	10	20
σ_{ex}/σ_{ey}	2	4	8

*Nominal anisotropy.

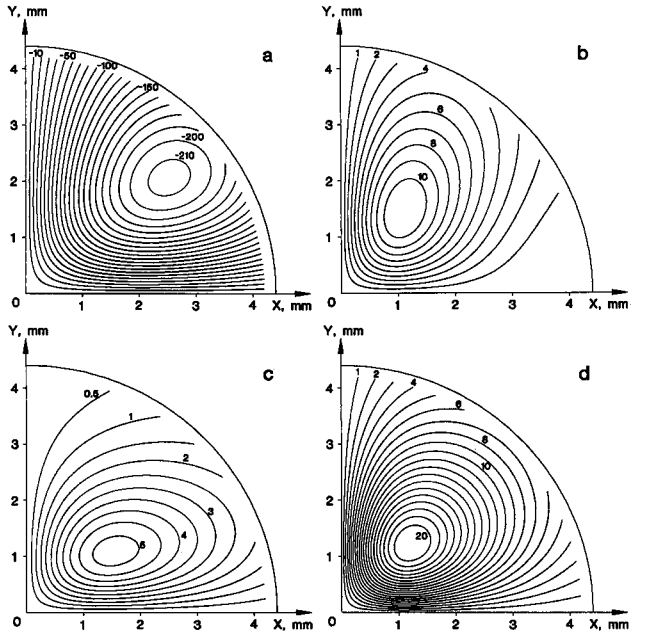

FIGURE 13 The isocontours of the normal component of the magnetic field (in nanoTesla) calculated 2 mm above the plane of the tissue. In *a* (nominal anisotropy) and *b* (reciprocal anisotropy) the current is cathodally applied with an extracellular electrode at the origin, with strength $I_o = 4$ mA. In *c* (nominal anisotropy) and *d* (reciprocal anisotropy), the current is applied at the origin with the intracellular electrode (+) and the extracellular electrode (−) carrying equal and opposite currents with strength $I_o = 4$ mA/mm. The thickness of the sheet of tissue is 1 mm, so that the total applied current is 4 mA.

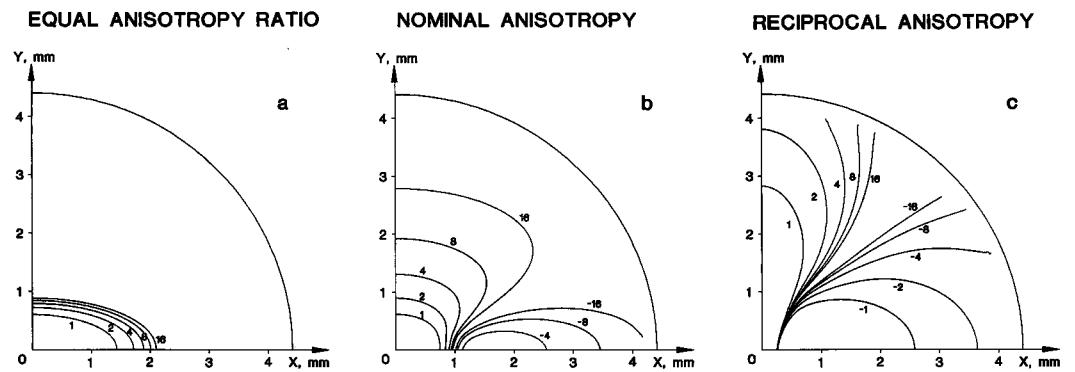

FIGURE 14 The +20 mV isopotential contour of the transmembrane potential for different amounts of injected current. The isopotential line is calculated for equal anisotropy ratios (*a*), nominal (*b*), and reciprocal conductivities (*c*). The current is applied extracellularly at the origin.

CONCLUSION

Cardiac tissue responds to an applied current by producing a surprisingly complicated distribution of potential and current. These unusual transmembrane potential distributions arise because of the different anisotropy ratios in the intracellular and interstitial space. Previous models, which either ignored anisotropy or assumed the same anisotropy in the intracellular and interstitial space, did not predict these results. One of the most surprising results we obtain is that current injected into the tissue at the cathode produces both depolarization and hyperpolarization. Although we have studied only a two-dimensional model, we expect that these results will carry over into three dimensions, where even more unusual current patterns might be produced. It is important that these theoretical predictions be experimentally verified. A sensitive experimental technique to test these predictions is to measure the magnetic field.

This work was supported by National Institute of Health grants NS19794, NS24751 and HL36724 and by grants from the Whitaker Foundation and the American Heart Association, Tennessee Affiliate. Partial support for the computing facilities was provided by the College of Arts and Sciences, Vanderbilt University.

Received for publication 29 August 1988 and in final form 3 January 1989.

REFERENCES

1. Eisenberg, R. S., V. Barcilon, and R. T. Mathias. 1979. Electrical properties of spherical syncytia. *Biophys. J.* 25:151–180.
2. Peskoff, A. 1979. Electric potential in three-dimensional electrically syncytial tissues. *Bull. Math. Biol.* 41:163–181.
3. Roth, B. J. 1987. Longitudinal resistance in strands of cardiac muscle. Ph.D. thesis. Vanderbilt University, Nashville, TN.
4. Tung, L. 1978. A bi-domain model for describing ischemic myocardial d-c potentials. Ph.D. thesis. Massachusetts Institute of Technology, Cambridge, MA.
5. Miller, W. T., III, and D. B. Geselowitz. 1978. Simulation studies of the electrocardiogram, I. The normal heart. *Circ. Res.* 43:301–315.
6. Geselowitz, D. B., and W. T. Miller III. 1983. A bidomain model for anisotropic cardiac muscle. *Ann. Biomed. Eng.* 11:191–206.
7. Plonsey, R., and R. C. Barr. 1982. The four-electrode resistivity technique as applied to cardiac muscle. *IEEE Trans. Biomed. Eng.* 29:541–546.
8. Muler, A. L., and V. S. Markin. 1977. Electrical properties of anisotropic nerve-muscle syncytia. I. Distribution of the electronic potential. *Biofizika.* 22:307–312.
9. Barr, R. C., and R. Plonsey. 1984. Propagation of excitation in idealized anisotropic two-dimensional tissue. *Biophys. J.* 45:1191–1202.
10. Plonsey, R., and R. C. Barr. 1984. Current flow patterns in two-dimensional anisotropic bisyncytia with normal and extreme conductivities. *Biophys. J.* 45:557–571.
11. Sepulveda, N. G., and J. P. Wikswo, Jr. 1987. Electric and magnetic fields from two-dimensional bisyncytia. *Biophys. J.* 51:557–568.
12. Roth, B. J., and J. P. Wikswo, Jr. 1986. A bi-domain model for the extracellular potential and the magnetic field of cardiac tissue. *IEEE Trans. Biomed. Eng.* 32:467–469.
13. Plonsey, R., and R. C. Barr. 1987. Interstitial potentials and their change with depth into cardiac tissue. *Biophys. J.* 51:547–555.
14. Roth, B. J., and F. L. H. Gielen. 1987. A comparison of two models for calculating the electrical potential in skeletal muscle. *Ann. Biomed. Eng.* 15:591–602.
15. Roberts, D. E., L. T. Hersh, and A. M. Scher. 1979. Influence of cardiac fiber orientation on wavefront voltage, conduction velocity, and tissue resistivity in the dog. *Circ. Res.* 44:701–712.
16. Woodbury, J. W., and W. E. Crill. 1961. On the problem of impulse conduction in the atrium. *In* Nervous Inhibition. Pergamon Journals Ltd., Oxford. 124–135.
17. Zienkiewicz, O. C. 1977. The Finite Element Method. McGraw-Hill Inc., London.
18. Hinton, E., and D. R. J. Owen. 1979. An Introduction to Finite Element Computations. Pineridge Press Limited, Swancea, UK.
19. Akin, J. E. 1982. Application and Implementation of Finite Element Methods. Academic Press, London.
20. Burnett, D. S. 1987. Finite Element Analysis. Addison-Wesley Publishing Co., Reading, MA.
21. Press, W. H., B. P. Flannery, S. A. Teukolsky, and W. T. Vetterling. 1986. Numerical Recipes. Cambridge University Press, Cambridge, MA. 449–453.
22. Wikswo, J. P., Jr., H. A. Kopelman, and D. M. Roden. 1985. Cardiac excitability and space constants measured *in vivo* using the virtual cathode effect. *Circulation.* 72:III-3.
23. Wikswo, J. P., Jr., J. P. Barach, W. Altmeier, and D. M. Roden. 1988. Measurements and modeling of virtual cathode effects in cardiac muscle. *Proc. World Congr. Med. Phys. Biomed. Eng.* 33(Suppl. I):232.
24. Wikswo, J. P., Jr. 1988. High resolution measurements of biomagnetic fields. *In* Advances in Cryogenic Engineering. R. W. Fast, editor. Plenum Publishing Corp., 107–116.